Nano Research
2019, 12(5): 1199–1206

ISSN 1998-0124 CN 11-5974/O4
https://doi.org/10.1007/s12274-019-2382-z

Research Article

A cross-linked polyacrylamide electrolyte with high ionic conductivity for compressible supercapacitors with wide temperature tolerance

Xuting Jin, Guoqiang Sun, Guofeng Zhang, Hongsheng Yang, Yukun Xiao, Jian Gao, Zhipan Zhang (✉), and Liangti Qu (✉)

Key Laboratory of Photoelectronic/Electrophotonic Conversion Materials, Key Laboratory of Cluster Science, Ministry of Education of China, School of Chemistry, Beijing Institute of Technology, Beijing 100081, China

Received: 12 January 2019 / **Revised:** 20 February 2019 / **Accepted:** 12 March 2019

ABSTRACT

The development of compressible supercapacitors (SCs) that is tolerant to wide temperature range has been severely hindered due to the poor ionic conductivity and absence of extra functions in conventional polymer electrolytes. Herein, a highly conductive and compressible hydrogel polyelectrolyte has been prepared from polyacrylamide cross-linked by methacrylated graphene oxide (MGO-PAM) and the polyelectrolyte can maintain its excellent elasticity at –30 °C as well as its original shape at 100 °C. As a result, the SC based on the MGO-PAM polyelectrolyte outperformed those fabricated with the conventional poly(vinyl alcohol) (PVA)/H_2SO_4 electrolyte over a wide temperature window between –30 and 100 °C. Meanwhile, the device shows an excellent cycling stability (capacitance retention of 93.3% after 8,000 cycles at –30 °C and 76.5 % after 4,000 cycles under 100 °C) and a reversible compressibility (a high capacitance retention of 94.1% under 80% compression). Therefore, the MGO-PAM polyelectrolyte enables the fabrication of compressible SCs with a wide operating temperature, rendering new insights for developing next-generation robust and multifunctional energy-storage devices.

KEYWORDS

ionic conductivity, compressibility, wide temperature tolerance, supercapacitors, polyacrylamide electrolyte

1 Introduction

Supercapacitors (SCs) have attracted a lot of research interests due to their merits of high power density and long cycle life [1–5]. As an indispensable component of SCs, the electrolyte plays an important role in determining the electrochemical performance of the devices. Currently, conventional poly(vinyl alcohol) (PVA)-based electrolytes, such as PVA/LiCl, PVA/KOH, PVA/H_3PO_4 and PVA/H_2SO_4, have been widely used in flexible SCs [6–9]. However, these polymer electrolytes are only of low ionic conductivity of ~ 2.5 S·m^{-1} [10–13] and lack of other functions, including compressibility and stretchability, in developing multifunctional SCs. Recently, new polyelectrolytes of polyacrylic acid/vinyl hybrid silica nanoparticles and polyacrylamide (PAM)/ vinyl hybrid silica nanoparticles have been applied to fabricate self-healing, compressible and stretchable SCs, [14, 15] but their conductivity (1.7 S·m^{-1}) was even lower than that of the PVA/H_2SO_4 electrolyte, leading to a narrow electrochemical window of 0–0.6 V and a low energy density. To solve this problem, more conductive hydrogel electrolytes such as PVA-based borax/KCl hydrogel electrolyte [16], PAM/LiCl electrolyte [17], and copolymer comprising of vinylimidazole and hydroxypropyl acrylate/H_2SO_4 [18] have been prepared and the maximum ionic conductivity could reach 8.1 S·m^{-1}. However, these hydrogel electrolytes usually contain a massive amount of water, which inevitably freeze and significantly lose their conductivity below 0 °C. Consequently, SCs assembled with these hydrogel electrolytes only operate properly around room temperature, suffering a severe loss in flexibility and device capacitance below –10 °C and thus limiting their applications in cold regions [19–21]. Alternatively, ionic liquids have been employed as electrolytes to improve the temperature tolerance of SCs [22–24]. Unfortunately, ionic liquids display high viscosity and poor ionic conductivity at low temperatures [25–27] and their hygroscopicity demands special cares in device fabrication [22, 28, 29]. Furthermore, it is very difficult to fabricate SCs with multifunctional property such as stretchability or compressibility by using ionic liquids as these electrolytes are neither stretchable nor elastic. Therefore, PVA/H_2SO_4 remains as the most widely used hydrogel electrolyte in flexible SCs to date, [17, 26, 30–35] but it tends to flow at 100 °C and impairs its usage under high temperatures [12]. In recent years, many research groups have relied on compressible electrodes (superelastic graphene foam monoliths as structural buffer) [36], elastic substrates (such as commercial polyurethane sponge or melamine foam) [37, 38] or hydrogel electrolytes [15, 39] to fabricate flexible and compressible energy storage devices. However, these devices generally have a poor temperature tolerance as ionic conductivities of these electrolytes seriously deteriorate when they do not operate at room temperature. Therefore, it is still challenging to find suitable polymer electrolyte that is highly conductive, compressible and stretchable in wide temperature range.

Recently, cross-linked polyacrylic acid derivatives and PAM hydrogel electrolytes have been used in flexible and high-performance energy storage devices such as Co_3O_4/Zn batteries and zinc-air batteries due to their good safety, high ionic conductivity and easiness to prepare [39–42]. Herein, we have designed and synthesized a new ethylene glycol-water (EG-water) hydrogel polyelectrolyte consisting of PAM cross-linked by methacrylated graphene oxide (MGO), which possesses a higher ionic conductivity (12.7 S·m^{-1}) than that of previously reported polyelectrolytes [10–18, 43], excellent elasticity as well as anti-freezing and anti-heating properties. When it was directly assembled with multi-wall carbon nanotube (MWCNT)-

Address correspondence to Zhipan Zhang, zhipan@bit.edu.cn; Liangti Qu, lqu@bit.edu.cn

polyaniline (M-PANI) films into a flexible SC, the device featured a high compressibility (94.1% capacity retention under 80% compression), wide operating temperature window (from −30 to 100 °C) and superior cycling stability (93.3% of capacitance retention after 8,000 cycles even at −30 °C). In addition, it delivered a high specific capacitance of 178.1 $F \cdot g^{-1}$ (at a current of 0.1 $A \cdot g^{-1}$), a maximum energy density of 15.8 $Wh \cdot kg^{-1}$ and a power density of 1,511.0 $W \cdot kg^{-1}$, respectively. More importantly, no matter under the low temperature of −30 °C or the high temperature of 100 °C, the device retained considerably higher capacitance than those fabricated with the widely-used PVA/H_2SO_4 electrolyte.

2 Experimental

2.1 Synthesis of the MGO-PAM polyelectrolyte

Graphene oxide (GO) and MGO were synthesized according to our previous report [44–46]. A typical fabrication procedure of MGO-PAM was described below. In brief, 20 mL MGO aqueous solution (0.6 $mg \cdot mL^{-1}$) was first prepared by ultrasonication at 0 °C before 5.2 g acrylamide (AM) monomers (Acros Organics) was slowly added. Subsequently, 5 μL N,N,N',N'-tetramethyl-ethylenediamine (TMED) catalysts and 0.02 mg ammonium persulfate (APS) (Sigma-Aldrich) initiators were added to initiate the free-radical polymerization under stirring at 0 °C. Then, the reaction solution was quickly poured in glass vessels and after sealing, the polymerization continued at 45 °C for 48 h to form the hydrogel. Finally, the obtained hydrogel was thoroughly dried at 50 °C. The MGO-PAM polyelectrolyte was obtained by soaking the dried gel in a 10 wt.% glycol/water (v:v = 1:1) solution of sulfuric acid for 72 h to achieve the equilibrated state. The swelling ratio of the prepared MGO-PAM polyelectrolyte was 1,500 wt.% and the water content was about 711.7% of the weight of the dried gel. It is noted that MGO-PAM polyelectrolytes with different swelling ratios and proton contents could be prepared by controlling the soaking time in the glycol/water solution of sulfuric acid. Similarly, the pure PAM polyelectrolyte was also prepared according to the above method.

2.2 Synthesis of the PVA/H_2SO_4 polyelectrolyte

The PVA/H_2SO_4 polyelectrolyte was prepared according to previously reported works [12, 26, 30–35, 43]. Briefly, 6 g PVA powder was added into 60 mL 10 wt.% aqueous solution of H_2SO_4 and the solution was stirred at 80 °C until it became transparent to yield the polyelectrolyte.

2.3 Fabrication of flexible SCs

M-PANI films were prepared by first immersing MWCNT films (Chengdu Organic Chemicals Co. Ltd., Chinese Academy of Sciences) in a mixed solution of sulfuric acid (1 M) and aniline monomer (0.1 M, Alfa Aesar) and electrodepositing PANI on MWCNT films via a cyclic voltammetry (CV) method (potential range of 0–1 V, 50 cycles, scan rate is 100 $mV \cdot s^{-1}$) on a CHI 760E electrochemical workstation with a conventional three-electrode setup (Pt and saturated calomel electrode served as the counter electrode and reference electrode, respectively) [47]. Flexible SCs were directly assembled by sandwiching the MGO-PAM polyelectrolyte (~ 3 mm in thickness) between two M-PANI films. Polydimethylsiloxane (PDMS) was used to encapsulate the devices for measuring the electrochemical performance in a wide temperature range of −30 to 100 °C.

3 Results and discussion

Figure 1(a) summarizes the synthesis of the MGO-PAM polyelectrolyte. GO and 3-(trimethoxysilyl)propyl methacrylate (MPS) reacted to form the MGO with unsaturated double bonds. As the pure PAM exhibits a poor compressibility and stretchability, it was grafted onto the MGO for better mechanical properties. Therefore, the MGO-PAM hydrogel was prepared by polymerizing the MGO with AM monomers in the presence of TMED as the catalyst and APS as the initiator. As shown in Figs. S1 and S2 in the Electronic Supplementary Material (ESM), the structures of the MGO and MGO-PAM hydrogel were proven by Fourier transform infrared spectroscopy (FTIR), Raman spectroscopy, X-ray diffraction (XRD), X-ray photoelectron spectroscopy (XPS), and scanning electron microscopy (SEM). In particular, the well-known D band (1,349 cm^{-1})

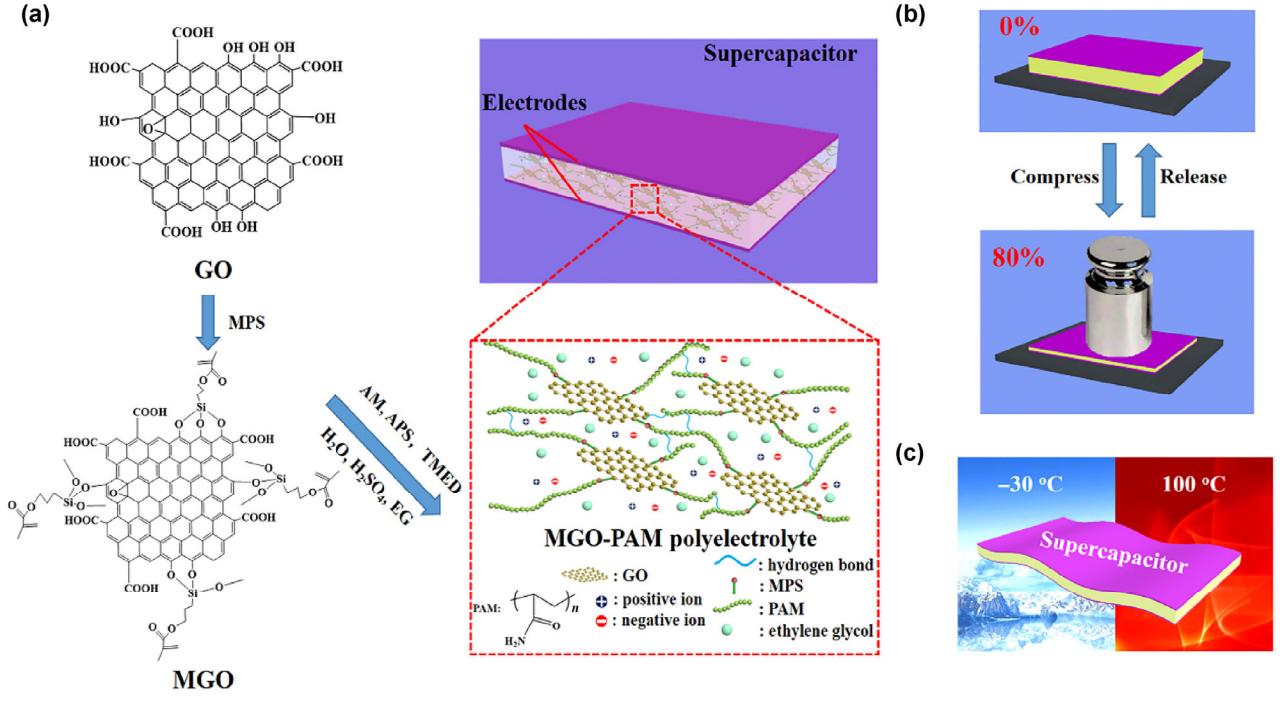

Figure 1 (a) The MGO-PAM polyelectrolyte prepared by the polymerization reaction of MGO (cross-linking agent) and acrylamide (monomer) in the existence of ammonium persulfate (initiator), TMED (catalyst), ethylene glycol, and sulfuric acid (proton source), and the SC assembled with two M-PANI film electrodes located directly on each side of the MGO-PAM polyelectrolyte. (b) Schematic of the SC with reciprocating compression ratio from 0% to 80%. (c) Anti-freezing and anti-heating performance illustration of the fabricated SC at a wide range of temperature from −30 to 100 °C.

and G band (1,597 cm^{-1}) of GO were discernible in the Raman spectroscopy of the dried MGO-PAM gel and the intensity ratio of the D/G band remained unchanged (Fig. S2(c) in the ESM), suggesting the retention of original GO moiety. Meanwhile, diffraction peaks originated from interlayer stacking at 2θ of ~ 10° in GO and MGO were absent in the MGO-PAM hydrogel (Fig. S2(d) in the ESM), implying a homogeneous dispersion of MGO sheets in the MGO-PAM hydrogel. Compared to the pure PAM, the higher glass transition temperature (T_g) observed in the MGO-PAM (101 °C vs. 94.1 °C) was associated with its restricted polymer chain motion due to the formation of cross-linked structure [48]. Therefore, the MGO played an important role in reinforcing mechanical properties via its covalently binding to PAM chains and acted as effective cross-linkers to dissipate external strain energy under deformations. The dried MGO-PAM gel was soaked in an EG/water (w:w = 1:1) solution of sulfuric acid to yield the MGO-PAM polyelectrolyte tolerant of large temperature variations [49–51]. Sulfuric acid supplied abundant protons to the polyelectrolyte and a high ionic conductivity of 12.7 $S{\cdot}m^{-1}$ was obtained. In addition, EG formed a glassy state with water to prevent ice crystallization below 0 °C [49] and greatly extended the operating temperature of the polyelectrolyte toward low temperatures [50, 51]. An elastic and temperature-tolerant SC was fabricated by sandwiching the MGO-PAM polyelectrolyte between two M-PANI film electrodes (Fig. 1(b)). Owing to the superelasticity of the polyelectrolyte, the assembled SC could be reversibly compressed up to a record high of 80% [15, 52]. More importantly, the device properly operated under wide temperature range from −30 and 100 °C, even maintaining its outstanding flexibility at −30 °C (Fig. 1(c)).

The excellent mechanical properties of the device originated from the MGO-PAM polyelectrolyte. As shown in Fig. 2(a), while the pure PAM polyelectrolyte was poor in mechanical strength, the MGO-PAM polyelectrolyte showed high elasticity (80% compression ratio) and stretchability (~ 480% extension ratio) (Figs. 2(b) and 2(e), and Fig. S4 in the ESM), mainly due to the formation of cross-linked polymer chains and extended hydrogen bond networks therein. Compared to the freeze-dried pure PAM, the wall between individual pores in the MGO-PAM gel was considerably thicker (Fig. S5 in the ESM), supporting its swelling in aqueous solution for a long period of time without structural collapse. In addition, as the MGO-PAM polyelectrolyte was rich in hydrogen bonds that interconnected cross-linked polymer chains, in the event that these hydrogen bonds broke under external stress, new hydrogen bonds could instantly form and reconnect polymer chains to evenly disperse energy across the whole polymer network (Fig. S6 in the ESM). As expected, the compression stress of the MGO-PAM electrolyte improved with the increasing MGO content (Fig. S7 in the ESM). In current work, an MGO content of 0.23 wt.% was chosen and its swelling ratio was 1,500 wt.% when the dried gel was soaked for 72 h in a 10 wt.% EG/water (v:v = 1:1) solution of sulfuric acid (see Experimental section for details). As shown in Fig. 2(f), the MGO-PAM polyelectrolyte could be repetitively compressed to 80% of its original height and resistant to a maximum external pressure of 150.4 kPa for 500 cycles, proving its stable elasticity. Additionally, the MGO-PAM polyelectrolyte remained fully elastic and flexible at −30 °C (Fig. 2(c) and Movie ESM1). In comparison, the conventional PVA/H_2SO_4 electrolyte was completely frozen into a stiff block at −20 °C (Fig. 2(d)). More importantly, the MGO-PAM electrolyte remained highly compressible after heated at 100 °C for 30 min (Fig. S8 in the ESM), suggesting its good water retention capacity due to the presence of strong EG–water interactions [53]. The SEM image in Fig. 2(g) shows the existence of plentiful micropores in the lyophilized MGO-PAM hydrogel and such a highly porous structure would facilitate unimpeded diffusions of electrolyte species. Meanwhile, the ionic conductivity of the prepared MGO-PAM polyelectrolyte reached 12.7 $S{\cdot}m^{-1}$, setting a new benchmark for electrolytes used in compressible SCs (Fig. 2(h)).

The impressive electrical, mechanical and thermal properties of the MGO-PAM polyelectrolyte are highly desirable in the design of flexible SCs. To utilize the high conductivity of MWCNT films together with the pseudocapacitive nature of PANI [54–57], we chose flexible M-PANI films as electrode materials (in Fig. 3(a)) for high-performance SCs. As shown in Figs. 3(b) and 3(c), PANI was uniformly electrodeposited on the surface of MWCNT films and the nature of M-PANI films was confirmed by Raman spectroscopy (Fig. S9 in the ESM). A monolithic SC was assembled by sandwiching

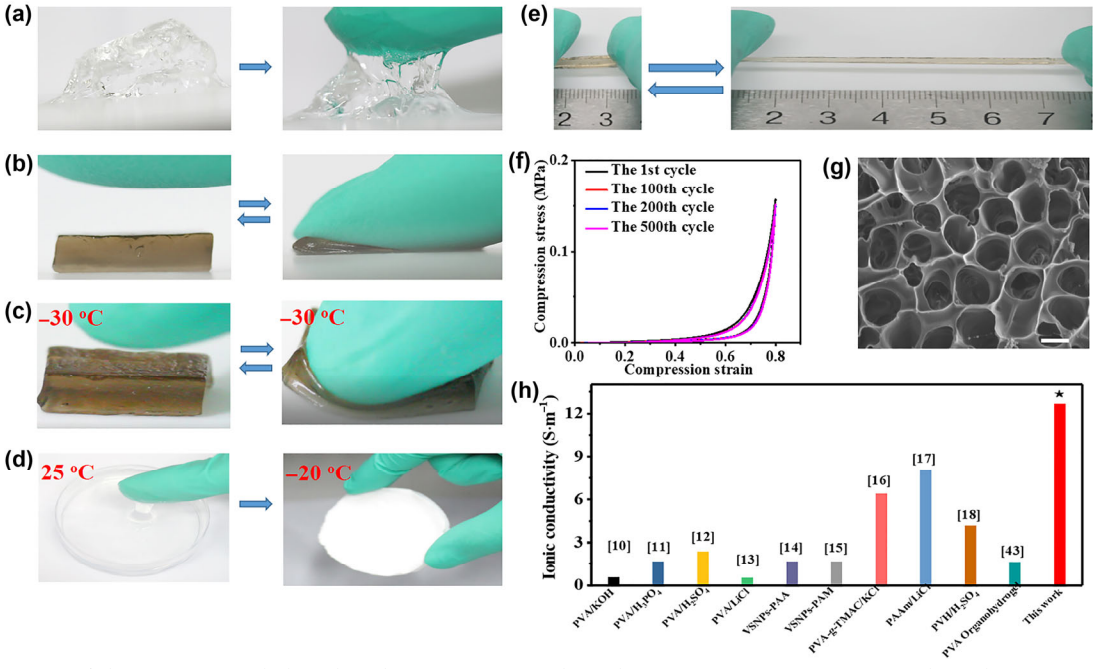

Figure 2 (a) The image of the pure PAM polyelectrolyte showing a poor mechanical property. Demonstration on mechanical properties of the MGO-PAM polyelectrolyte (b) at room temperature and (c) at −30 °C. (d) A stiff block of PVA/H_2SO_4 frozen at −20 °C. (e) Stretchable property of MGO-PAM polyelectrolyte. (f) Cyclic stress–strain curves at 80% compression strain of MGO-PAM polyelectrolyte. (g) The SEM image of the freeze-dried MGO-PAM hydrogel. Scale bar: 10 μm. (h) Comparison of ionic conductivity of MGO-PAM polyelectrolyte to other reported polyelectrolytes [10–18, 43].

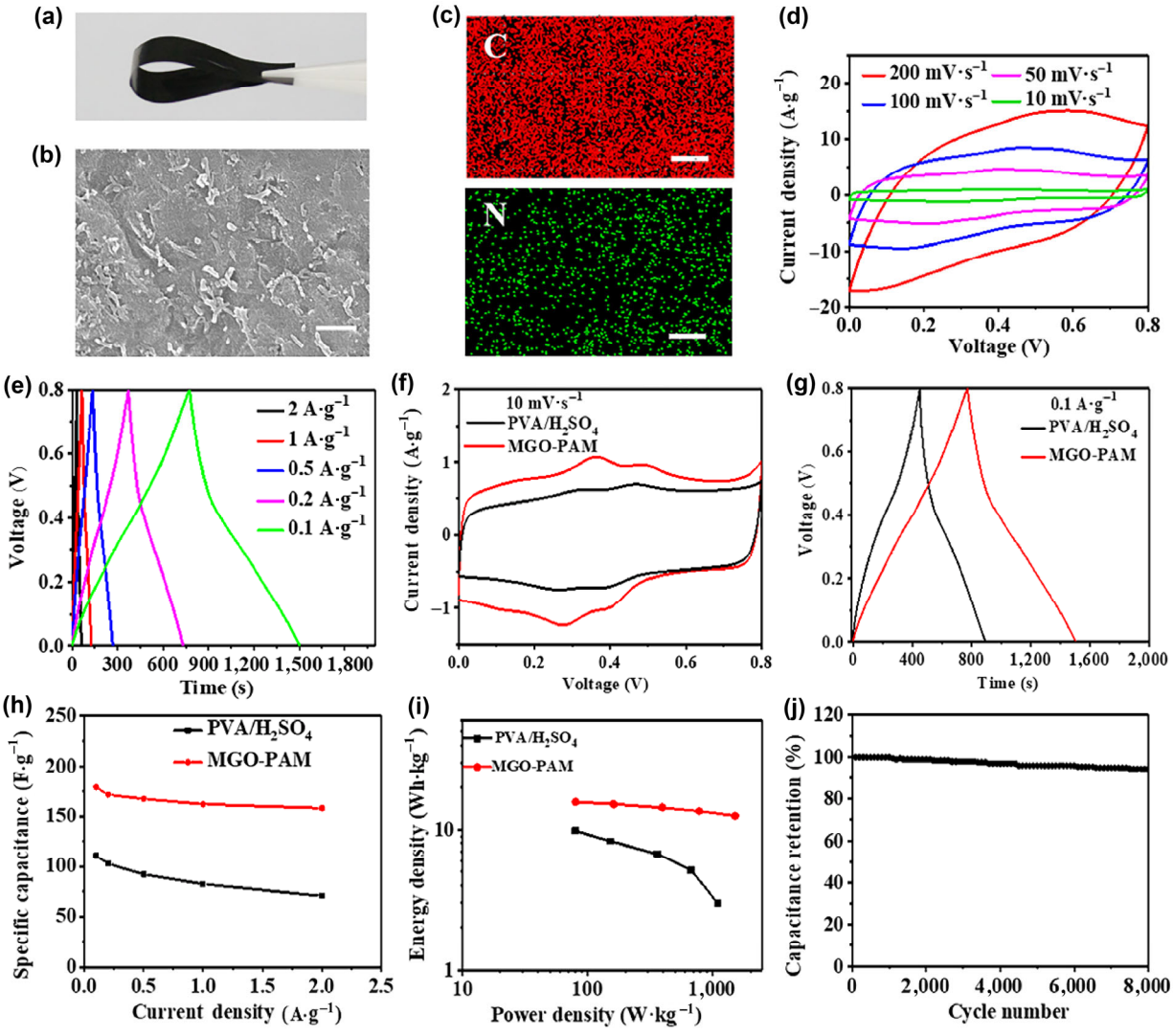

Figure 3 (a) Photograph of flexible M-PANI film. (b) The SEM image and (c) corresponding EDS mapping of M-PANI film. Scale bar: 1 μm. (d) CV curves at variable scan rates from 10 to 200 mV·s^{-1}, and (e) GCD profiles at various current densities from 0.1 to 2 A·g^{-1} of the SCs with MGO-PAM polyelectrolytes. (f) CV curves at the scan rate of 10 mV·s^{-1}, (g) GCD profiles at the current densities of 0.1 A·g^{-1}, (h) rate performance, and (i) Ragone plot (energy density vs. power density) of the SCs using MGO-PAM polyelectrolyte and PVA/H_2SO_4 electrolyte. (j) Cycling performance of the SCs with MGO-PAM polyelectrolyte at a current density of 2 A·g^{-1}.

the MGO-PAM polyelectrolyte between two M-PANI films. CV curves and galvanostatic charge/discharge (GCD) curves of the device are shown in Figs. 3(d) and 3(e), respectively. Two pairs of redox peaks were particularly apparent at low scan rates of 10 and 50 mV·s^{-1} (Fig. 3(d) and Fig. S10 in the ESM), which originated from redox transitions between polaronic emeraldine (a conducting state) and leucoemeraldine (a semiconducting state) forms of PANI [58–60]. With the scan rate increasing from 10 to 200 mV·s^{-1}, the CV curve became slightly distorted and the above-mentioned redox peaks were less discernible due to the shorter ion diffusion time at high scan rates [58]. Typical nonlinear GCD curves were found in the device owing to the presence of PANI (Fig. 3(e)) and its specific capacitance reached 178.1 F·g^{-1} at a current density of 0.1 A·g^{-1} even without using additional current collectors for device optimization. In addition, the conventional PVA/H_2SO_4 electrolyte was also used to fabricate a control device by using the same M-PANI electrodes. As shown in Figs. 3(f) and 3(g), the device based on the prepared MGO-PAM polyelectrolyte exhibited considerably higher capacitive performance than the control device, featuring a lower electrochemical impedance as well (Fig. S11 in the ESM). When the discharge current density increased to 2 A·g^{-1}, the specific capacitance of the device with the MGO-PAM polyelectrolyte slightly decreased to 158.3 F·g^{-1}, while that of the control device considerably dropped to 70.5 F·g^{-1} under the same condition (Fig. 3(h)). Consequently, the SC with the MGO-PAM polyelectrolyte delivered a maximum energy density of 15.8 Wh·kg^{-1} and power density of 1,511.0 W·kg^{-1} (Fig. 3(i)), which were significantly higher than those of the device using PVA/H_2SO_4 polyelectrolyte (maximum energy density of 9.83 Wh·kg^{-1} and power density of 1,100.5 W·kg^{-1}). More importantly, the SC using the MGO-PAM polyelectrolyte displayed high capacitance retention of 94.5% at a current density 2 A·g^{-1} after 8,000 consecutive cycles, validating its satisfactory long-term electrochemical stability (Fig. 3(j)).

Due to the high ionic conductivity of the MGO-PAM polyelectrolyte, the electrochemical performance of the assembled SC was barely affected by the thickness of the polyelectrolyte (Fig. S12 in the ESM). Therefore, CV and GCD curves of the compressed device only showed marginal changes (Fig. S13(a) in the ESM and Fig. 4(a)). For instance, when the device was compressed to 60% and 80%, it maintained 97.7% and 94.6% of the original capacitance, respectively (Fig. 4(b)). In addition, after 100 compressing/releasing cycles at a maximum compression ratio of 80%, the device showed almost unchanged CV and GCD curves (Fig. S13(b) in the ESM and Fig. 4(c)) and retained 97.1% of its original capacitance (Fig. 4(c)), demonstrating

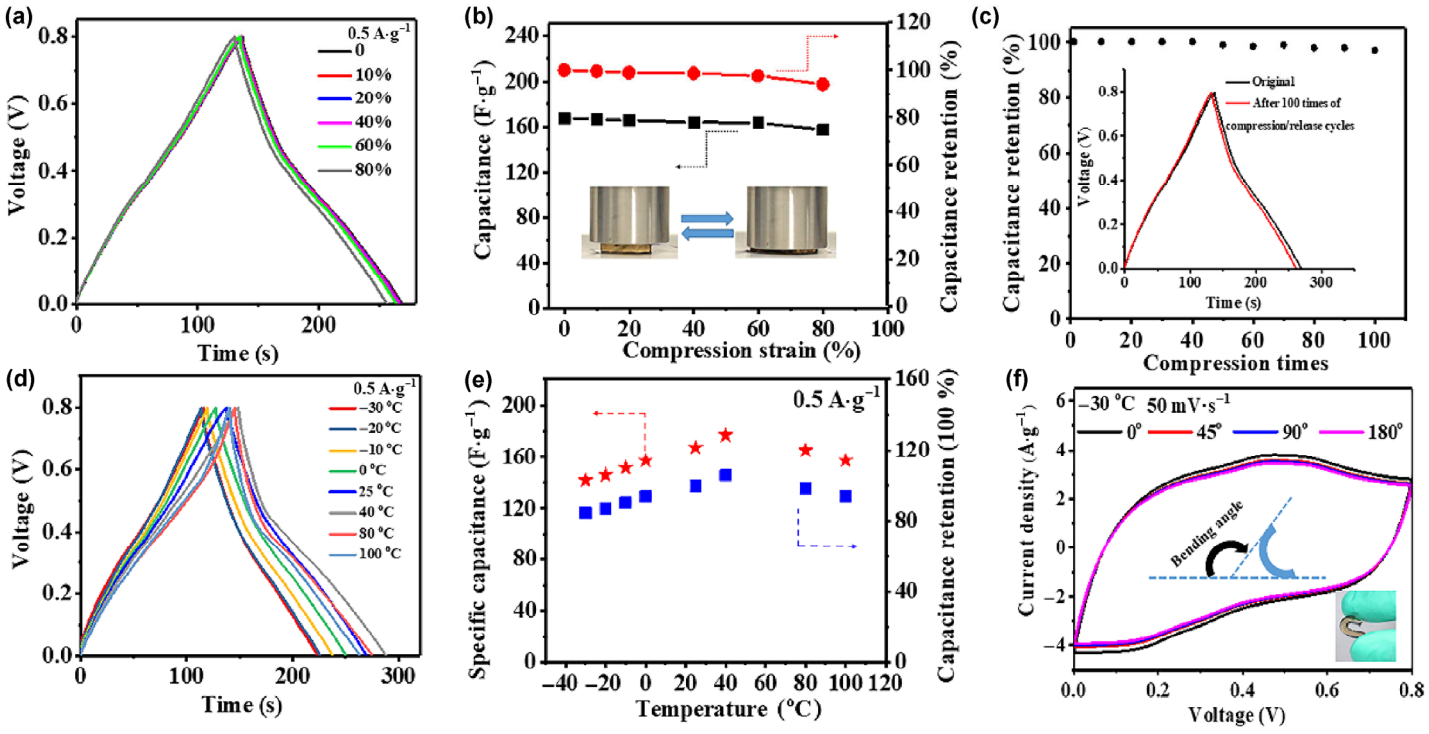

Figure 4 (a) GCD curves and (b) specific capacitance and capacitance retention of the SCs with MGO-PAM polyelectrolyte under different compression ratios. (c) GCD curves and capacitance retention of the SCs with MGO-PAM polyelectrolyte after 100 compression/release cycles at the current density of 0.5 A·g^{-1} at a maximum compression ratio of 80%. (d) GCD curves and (e) specific capacitance and capacitance retention of fabricated SCs by MGO-PAM polyelectrolyte at the different temperature. (e) CV curves of SCs with the different bending angles at −30 °C.

its outstanding compressibility. Thermally, the device could properly operate at the low temperature of −30 °C and high temperature of 100 °C. When the temperature rose from −30 to 100 °C, both the area within CV curves and the discharge time in GCD curves first increased and then decreased (in Fig. S14(a) in the ESM and Fig. 4(e)). As shown in Fig. 4(e), the specific capacitance of the device was 141.7 F·g^{-1} (at −30 °C) and 157.2 F·g^{-1} (at 100 °C), respectively, corresponding to 84.7% and 94% of its original value at room temperature (Fig. 4(e)). Despite of the small decrease in the capacitance, the nearly vertical line at low frequencies in the electrochemical impedance spectrum confirmed the ideal capacitive behavior of the device between −30 and 100 °C (Fig. S14(b) in the ESM). All these results unambiguously proved the excellent temperature tolerance of the device due to the high ionic conductivity at low or high temperatures (Fig. S14(c) in the ESM). Under −30 °C, no significant changes occurred in the CV curves when the device was bent between 45° to 180° (Fig. 4(i)), confirming the excellent mechanical flexibility and stability of the device that were never seen in other SCs at this temperature. The CV curve and GCD profiles of the device were further compared with those of the device made with the PVA/H_2SO_4 polyelectrolyte at −30 °C (Figs. 5(a) and 5(b)). Obviously, the capacitance (141.7 F·g^{-1} at 0.5 A·g^{-1}) of the device with the MGO-PAM electrolyte was considerably higher than that (68 F·g^{-1} at 0.5 A·g^{-1}) of the SCs with the PVA/H_2SO_4 polyelectrolyte, which was mainly attributed to the presence of EG that prevented the MGO-PAM electrolyte from frozen as the PVA/H_2SO_4 polyelectrolyte. In addition, both devices also were tested at 100 °C. As shown in Figs. 5(c) and 5(d), the electrochemical performance of the PVA/H_2SO_4 polyelectrolyte was far inferior to that of the MGO-PAM polyelectrolyte, presumably due to its tendency to flow and reshape [12]. In contrast, the cross-linked structure and the presence of EG in the MGO-PAM polyelectrolyte enhanced the high temperature tolerance of the device. Therefore, even at the high temperature of 100 °C, the fabricated device based on the MGO-PAM electrolyte retained the capacitance of 157.2 F·g^{-1} at 0.5 A·g^{-1}, far exceeding that (33.68 F·g^{-1} at 0.5 A·g^{-1}) of SCs with PVA/H_2SO_4 electrolytes. Overall, the capacitance retention was 93.3% at a current density 2 A·g^{-1} after 8,000 consecutive cycles under −30 °C (Fig. 5(e)) and 76.5 % after 4,000 cycles under 100 °C (Fig. 5(f)), respectively, demonstrating its good long-term electrochemical stability under wide range of temperature. It is noted that the capacitance retention increased after 2,000 cycles under 100 °C and this was presumably related to the inevitable solvent loss during long term operations at this high temperature even though the MGO-PAM electrolyte could retain water fairly well. The evaporation of EG and/or water led to an increase of acid concentration in the electrolyte, and in a certain range, this would improve the ionic conductivity of the polyelectrolyte and the capacitance retention as well. However, with a further loss of solvent molecules, the ionic conductivity of the electrolyte eventually dropped and the electrochemical performance of supercapacitor decreased to 76.5% after 4,000 cycles.

The flexible SCs were connected in series or in parallel to reach a higher voltage or current. As shown in Fig. 6(a), the potential range increased linearly with the number of SCs in series and a discharge potential of 2.4 V could be obtained when three SCs were connected in series (Fig. 6(b)). As a result, the calculator was fully functional when powered by two SCs and its screen brightness remained unchanged even under a load of 500 g (Fig. 6(c) and Movie ESM2), validating the excellent compressibility of both SCs. Remarkably, two identical SCs connected in series could still power the calculator with all functions available when they were placed in ice water (0 °C) (Fig. 6(d) and Movie ESM3) or on a hot plate (100 °C) (Fig. 6(e) and Movie ESM4). Moreover, three in-series SCs competently lighted up a red light-emitting diode (LED) under the load of 500 g, in the ice water (0 °C) or on the hot plate (Fig. S15 in the ESM and Movie ESM5). Therefore, the utilization of the MGO-PAM polyelectrolyte permitted the assembly of compressible SCs (up to 80%) tolerant of a wide temperature range from −30 to 100 °C, and as summarized in Table 1, the performance of the device was superior to those of the flexible SCs reported previously in terms of compressibility and temperature resistance [15, 19, 23, 61–66].

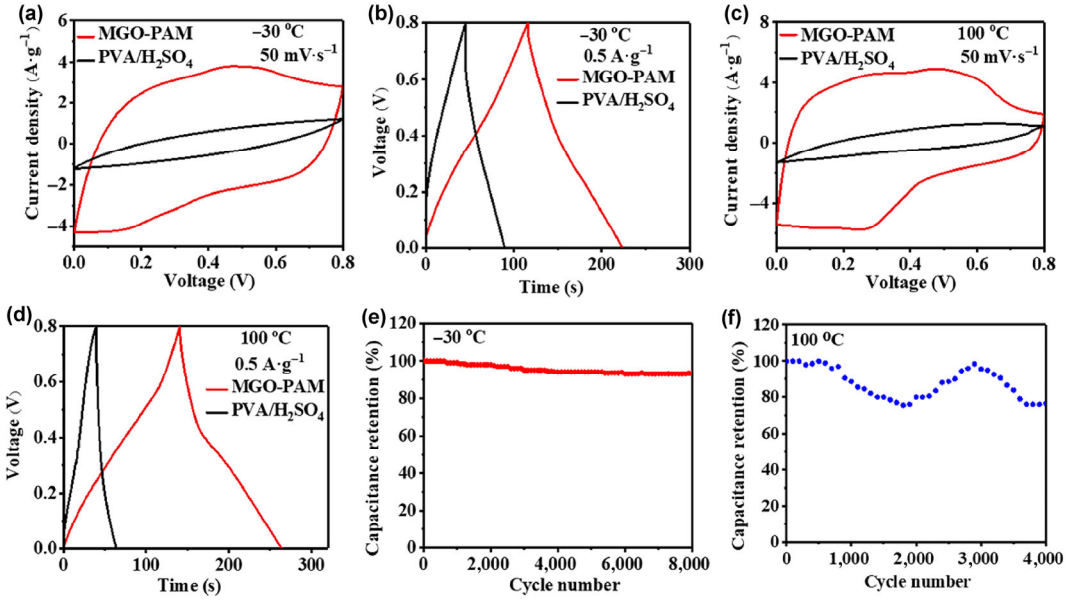

Figure 5 (a) CV curves and (b) GCD profiles of the devices with MGO-PAM polyelectrolyte and PVA/H_2SO_4 under −30 °C. (c) CV curves and (d) GCD profiles of the devices with MGO-PAM polyelectrolyte and PVA/H_2SO_4 under 100 °C. Cycling performance of the SCs with MGO-PAM polyelectrolyte at a current density of 2 A·g^{-1} in the temperature of (e) −30 and (f) 100 °C.

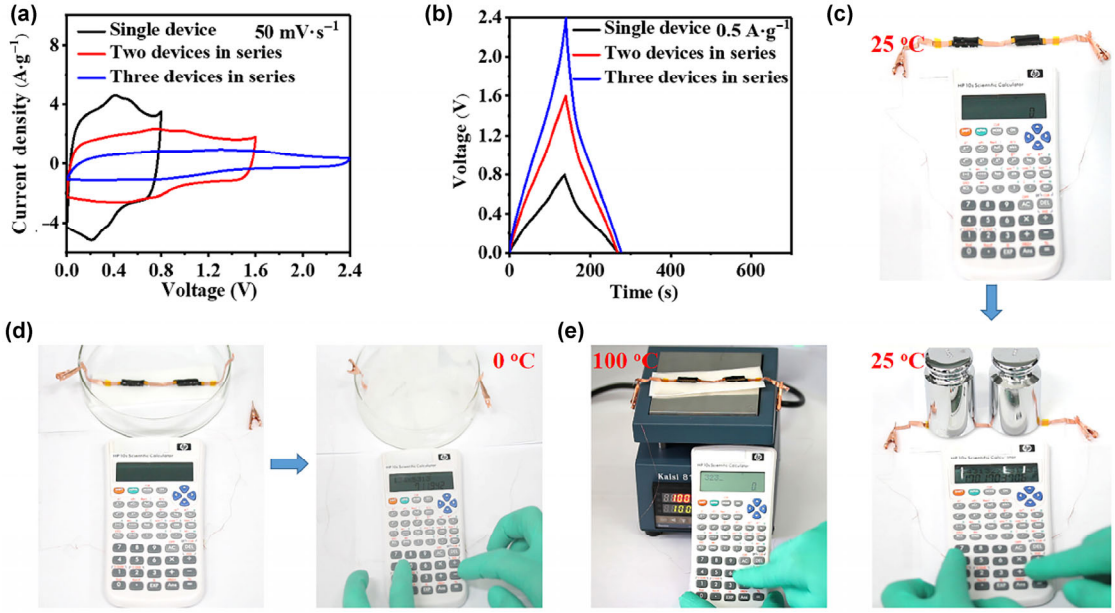

Figure 6 (a) The CV curves at the scan rate of 50 mV·s^{-1} and (b) GCD profiles at the current densities of 0.5 A·g^{-1} of a single SC, two SCs in series and three SCs in series. Photographs showing two series-connected SCs that could power a commercial calculator (c) under two load weights of 500 g, (d) in the ice water (0 °C) and (e) at the heating equipment of 100 °C.

Table 1 Summary of compressible SCs with temperature tolerance

Reference	Maximum compression of SC	Temperature tolerance of SCs (°C)
This work	80%	−30 to 100
[15]	50%	N/A
[19]	N/A	−15 to 25
[23]	N/A	−30 to 55
[61]	75%	N/A
[62]	50%	N/A
[63]	60%	N/A
[64]	60%	N/A
[65]	60%	N/A
[66]	80%	N/A

4 Conclusions

In summary, we have prepared a new type of MGO-PAM polyelectrolyte with excellent compressibility, high ionic conductivity as well as extreme temperature tolerance. The MGO-PAM polyelectrolyte could be used to directly fabricate the compressible SC with high capacitance retention of 94.1% under 80% compression. More importantly, the device stably operated within a wide temperature window from −30 to 100 °C, showing considerably higher capacitance than those fabricated with the widely-used PVA/H_2SO_4 electrolyte. The current work provides new insights into the development of temperature resistant SCs with high compressibility for practical applications in modern electronics such as flexible energy devices and soft robot systems.

Acknowledgements

We acknowledge the financial support from the National Key R&D Program of China (Nos. 2017YFB1104300 and 2016YFA0200200), the National Natural Science Foundation of China (Nos. 51673026, 51433005, and 21774015), NSFC-MAECI (No. 51861135202), Beijing Municipal Science and Technology Commission (Nos. Z161100002116022 and Z161100002116029).

Electronic Supplementary Material: Supplementary material (the SEM image and corresponding EDS mapping of MGO film; FTIR spectrum, XPS spectrum, Roman spectrum and XRD spectrum of MGO-PAM; T_g of MGO-PAM; the mechanical property of MGO-PAM polyelectrolyte and mechanism illustration of the stretchability and compressibility; CV curves at variable scan rates of SCs with MGO-PAM polyelectrolyte; CV curves, GCD curves, specific capacitance and EIS of the prepared SCs based on MGO-PAM polyelectrolyte with different thickness; the compression performance of SCs with MGO-PAM polyelectrolyte; GCD curves, EIS of the fabricated SCs by MGO-PAM polyelectrolyte at the different temperature; the ionic conductivity of MGO-PAM polyelectrolyte at the different temperature; photographs showing that three series-connected SCs could power a red light-emitting diode under the load weight, in the ice water and at the heating equipment) is available in the online version of this article at https://doi.org/10.1007/s12274-019-2382-z.

References

[1] Zhu, Y. W.; Murali, S.; Stoller, M. D.; Ganesh, K. J.; Cai, W. W.; Ferreira, P. J.; Pirkle, A.; Wallace, R. M.; Cychosz, K. A.; Thommes, M. et al. Carbon-based supercapacitors produced by activation of graphene. *Science* **2011**, *332*, 1537–1541.

[2] Kou, L.; Huang, T. Q.; Zheng, B. N.; Han, Y.; Zhao, X. L.; Gopalsamy, K.; Sun H. Y.; Gao, C. Coaxial wet-spun yarn supercapacitors for high-energy density and safe wearable electronics. *Nat. Commun.* **2014**, *5*, 3754.

[3] Yu, D. S; Goh, K.; Wang, H.; Wei, L.; Jiang, W. C.; Zhang, Q.; Dai, L. M.; Chen, Y. Scalable synthesis of hierarchically structured carbon nanotube–graphene fibres for capacitive energy storage. *Nat. Nanotechnol.* **2014**, *9*, 555–562.

[4] Lin, T. Q.; Chen, I. W.; Liu, F. X.; Yang, C. Y.; Bi, H.; Xu F. F.; Huang, F. Q. Nitrogen-doped mesoporous carbon of extraordinary capacitance for electrochemical energy storage. *Science* **2015**, *350*, 1508–1513.

[5] Yang, Y.; Huang, Q. Y.; Niu, L. Y.; Wang, D. R.; Yan, C.; She Y. Y.; Zheng, Z. J. Waterproof, ultrahigh areal-capacitance, wearable supercapacitor fabrics. *Adv. Mater.* **2017**, *29*, 1606679.

[6] Choi, C.; Kim, K. M.; Kim, K. J.; Lepró, X.; Spinks, G. M.; Baughman R. H.; Kim, S. J. Improvement of system capacitance via weavable superelastic biscrolled yarn supercapacitors. *Nat. Commun.* **2016**, *7*, 13811.

[7] Li, C.; Islam, M.; Moore, J.; Sleppy, J.; Morrison, C.; Konstantinov, K.; Dou, S. X.; Renduchintala, C.; Thomas, J. Wearable energy-smart ribbons for synchronous energy harvest and storage. *Nat. Commun.* **2016**, *7*, 13319.

[8] Lu, Z.; Foroughi, J.; Wang, C. Y.; Long H. R.; Wallace, G. G. Superelastic hybrid CNT/graphene fibers for wearable energy storage. *Adv. Energy Mater.* **2017**, *8*, 1702047.

[9] Li, L.; Zhang, J. B.; Peng, Z. W.; Li, Y. L.; Gao, C. T.; Ji, Y. S.; Ye, R. Q.; Kim, N. D.; Zhong, Q. F.; Yang, Y. et al. High-performance pseudocapacitive microsupercapacitors from laser-induced graphene. *Adv. Mater.* **2016**, *28*, 838–845.

[10] Yu, H. J.; Wu, J. H.; Fan, L. Q.; Xu, K. Q.; Zhong, X.; Lin Y. Z.; Lin, J. M. Improvement of the performance for quasi-solid-state supercapacitor by using PVA-KOH-KI polymer gel electrolyte. *Electrochim. Acta* **2011**, *56*, 6881–6886.

[11] Kufian, M. Z.; Majid S. R.; Arof, A. K. Dielectric and conduction mechanism studies of PVA-orthophosphoric acid polymer electrolyte. *Ionics* **2007**, *13*, 231–234.

[12] Fei, H. J.; Yang, C. Y.; Bao H.; Wang, G. C. Flexible all-solid-state supercapacitors based on graphene/carbon black nanoparticle film electrodes and cross-linked poly(vinyl alcohol)-H_2SO_4 porous gel electrolytes. *J. Power Sources* **2014**, *266*, 488–495.

[13] Lv, Q. Y.; Chi, K.; Zhang, Y.; Xiao, F.; Xiao, J. W.; Wang S.; Lohc, K. P. Ultrafast charge/discharge solid-state thin-film supercapacitors via regulating the microstructure of transition-metal-oxide. *J. Mater. Chem. A.* **2017**, *5*, 2759–2767.

[14] Huang, Y.; Zhong, M.; Huang, Y.; Zhu, M. S.; Pei, Z. X.; Wang, Z. F.; Xue, Q.; Xie X. M.; Zhi, C. Y. A self-healable and highly stretchable supercapacitor based on a dual crosslinked polyelectrolyte. *Nat. Commun.* **2015**, *6*, 10310.

[15] Huang, Y.; Zhong, M.; Shi, F. K.; Liu, X. Y.; Tang, Z. J.; Wang, Y. K.; Huang, Y.; Hou, H. Q.; Xie X. M.; Zhi, C. Y. An intrinsically stretchable and compressible supercapacitor containing a polyacrylamide hydrogel electrolyte. *Angew. Chem., Int. Ed.* **2017**, *56*, 9141–9145.

[16] Wang, Z. K.; Pan, Q. M. An omni-healable supercapacitor integrated in dynamically cross-linked polymer networks. *Adv. Funct. Mater.* **2017**, *27*, 1700690.

[17] Li, H. L.; Lv, T.; Li, N.; Yao, Y.; Liu K.; Chen, T. Ultraflexible and tailorable all-solid-state supercapacitors using polyacrylamide-based hydrogel electrolyte with high ionic conductivity. *Nanoscale* **2017**, *9*, 18474–18481.

[18] Liu, F. T.; Wang J. C.; Pan, Q. M. An all-in-one self-healable capacitor with superior performance. *J. Mater. Chem. A* **2018**, *6*, 2500–2506.

[19] Tao, F.; Qin, L. M.; Wang Z. K.; Pan, Q M. Self-healable and cold-resistant supercapacitor based on a multifunctional hydrogel electrolyte. *ACS Appl. Mater. Interfaces* **2017**, *9*, 15541–15548.

[20] Liu, M. J.; Wang S. T.; Jiang, L. Nature-inspired superwettability systems. *Nat. Rev. Mater.* **2017**, *2*, 17036.

[21] Abbas, Q.; Béguin, F. Sustainable carbon/carbon supercapacitors operating down to −40 °C in aqueous electrolyte made with cholinium salt. *ChemSusChem* **2018**, *11*, 975–984.

[22] Zhong, C.; Deng, Y. D.; Hu, W. B.; Qiao, J. L.; Zhang L.; Zhang, J. J. A review of electrolyte materials and compositions for electrochemical supercapacitors. *Chem. Soc. Rev.* **2015**, *44*, 7484–7539.

[23] Zang, X. B.; Zhang, R. J.; Zhen, Z.; Lai, W. H.; Yang, C.; Kang F. Y.; Zhu, H. W. Flexible, temperature-tolerant supercapacitor based on hybrid carbon film electrodes. *Nano Energy* **2017**, *40*, 224–232.

[24] Liu, W. W.; Yan, X. B.; Lang J. W.; Xue, Q. J. Effects of concentration and temperature of $EMIMBF_4$/acetonitrile electrolyte on the supercapacitive behavior of graphene nanosheets. *J. Mater. Chem.* **2012**, *22*, 8853–8861.

[25] Feng, L. X.; Wang, K.; Zhang, X.; Sun, X. Z.; Li, C.; Ge X. B.; Ma, Y. W. Flexible solid-state supercapacitors with enhanced performance from hierarchically graphene nanocomposite electrodes and ionic liquid incorporated gel polymer electrolyte. *Adv. Funct. Mater.* **2018**, *28*, 1704463.

[26] Lu, X. H.; Yu, M. H.; Wang, G. M.; Tong Y. X.; Li, Y. Flexible solid-state supercapacitors: Design, fabrication and applications. *Energy Environ. Sci.* **2014**, *7*, 2160–2181.

[27] Dou, Q. Y.; Lei, S. L.; Wang, D. W.; Zhang, Q. N.; Xiao, D. W.; Guo, H. W.; Wang, A. P.; Yang, H.; Li, Y. L.; Shi S. Q. et al. Safe and high-rate supercapacitors based on an "acetonitrile/water in salt" hybrid electrolyte. *Energy Environ. Sci.* **2018**, *11*, 3212–3219.

[28] Yamada, Y.; Usui, K.; Sodeyama, K.; Ko, S.; Tateyama Y.; Yamada, A. Hydrate-melt electrolytes for high-energy-density aqueous batteries. *Nat. Energy* **2016**, *1*, 16129.

[29] Dou, Q. Y.; Liu, L. Y.; Yang, B. J.; Lang J. W.; Yan, X. B. Silica-grafted ionic liquids for revealing the respective charging behaviors of cations and anions in supercapacitors. *Nat. Commun.* **2017**, *8*, 2188.

[30] Xu, Y. X.; Lin, Z. Y.; Huang, X. Q.; Liu, Y.; Huang Y.; Duan, X. F. Flexible solid-state supercapacitors based on three-dimensional graphene hydrogel films. *ACS Nano* **2013**, *7*, 4042–4049.

[31] Meng, C. Z.; Liu, C. H.; Chen, L. Z.; Hu, C. H.; Fan, S. S. Highly flexible and all-solid-state paperlike polymer supercapacitors. *Nano Lett.* **2010**, *10*, 4025–4031.

[32] Liu, D. Q.; Li, Q. W.; Zhao, H. Z. Electrolyte-assisted hydrothermal synthesis of holey graphene films for all-solid-state supercapacitors. *J. Mater. Chem. A* **2018**, *6*, 11471–11478.

[33] Li, P. P.; Jin, Z. Y.; Peng, L. L.; Zhao, F.; Xiao, D.; Jin, Y.; Yu, G. H. Stretchable all-gel-state fiber-shaped supercapacitors enabled by macromolecularly interconnected 3D graphene/nanostructured conductive polymer hydrogels. *Adv. Mater.* **2018**, *30*, 1800124.

[34] Hall, P. J.; Mirzaeian, M.; Fletcher, S. I.; Sillars, F. B.; Rennie, A. J. R.; Shitta-Bey, G. O.; Wilson, G.; Cruden, A.; Carter, R. Energy storage in electrochemical capacitors: Designing functional materials to improve performance. *Energy Environ. Sci.* **2010**, *3*, 1238–1251.

[35] Meng, Y. N.; Zhao, Y.; Hu, C. G.; Cheng, H. H.; Hu, Y.; Zhang, Z. P.; Shi G. Q.; Qu, L. T. All-graphene core-sheath microfibers for all-solid-state,

stretchable fibriform supercapacitors and wearable electronic textiles. *Adv. Mater*. **2013**, *25*, 2326–2331.
[36] He, D.; Song, L.; Lv, L. X.; Zhang, Z. P.; Qu, L. T. Superelastic air-bubbled graphene foam monoliths as structural buffer for compressible high-capacity anode materials in lithium-ion batteries. *Chem. Eng. J*. **2018**, *331*, 704–711.
[37] Wang, X. P.; Gao, J.; Cheng, Z. H.; Chen, N.; Qu, L. T. A responsive battery with controlled energy release. *Angew. Chem., Int. Ed*. **2016**, *55*, 14643–14647.
[38] Shao, C. X.; Xu, T.; Gao, J.; Liang, Y.; Zhao, Y.; Qu, L. T. Flexible and integrated supercapacitor with tunable energy storage. *Nanoscale* **2017**, *9*, 12324–12329.
[39] Ma, L. T.; Chen, S. M.; Pei, Z. X.; Huang, Y.; Liang, G. J.; Mo, F. N.; Yang, Q.; Su, J.; Gao, Y. H.; Zapien, J. A. et al. Single-site active iron-based bifunctional oxygen catalyst for a compressible and rechargeable zinc-air battery. *ACS Nano* **2018**, *12*, 1949–1958.
[40] Ma, L. T.; Chen, S. M.; Wang, D. H.; Yang, Q.; Mo, F. N.; Liang, G. J.; Li, N.; Zhang, H. Y.; Zapien, J. A.; Zhi, C. Y. Super-stretchable zinc-air batteries based on an alkaline-tolerant dual-network hydrogel electrolyte. *Adv. Energy Mater*. **2019**, 1803046.
[41] Li, H. F.; Liu, Z. X.; Liang, G. J.; Huang, Y.; Huang, Y.; Zhu, M. S.; Pei, Z. X.; Xue, Q.; Tang, Z. J.; Wang, Y. K. et al. Waterproof and tailorable elastic rechargeable yarn Zinc ion batteries by a cross-linked polyacrylamide electrolyte. *ACS Nano* **2018**, *12*, 3140–3148.
[42] Ma, L. T.; Chen, S. M.; Li, H. F.; Ruan, Z. H.; Tang, Z. J.; Liu, Z. X.; Wang, Z. F.; Huang, Y.; Pei, Z. X.; Zapien, J. A. et al. Initiating a mild aqueous electrolyte Co_3O_4/Zn battery with 2.2 V-high voltage and 5000-cycle lifespan by a Co(III) rich-electrode. *Energy Environ. Sci*. **2018**, *11*, 2521–2530.
[43] Rong, Q. F.; Lei, W. W.; Huang J.; Liu, M. J. Low temperature tolerant organohydrogel electrolytes for flexible solid-State supercapacitors. *Adv. Energy Mater*. **2018**, *8*, 1801967.
[44] Cheng, H. H.; Hu, Y.; Zhao, F.; Dong, Z. L.; Wang, Y. H.; Chen, N.; Zhang Z. P.; Qu, L. T. Moisture-activated torsional graphene-fiber motor. *Adv. Mater*. **2014**, *26*, 2909–2913.
[45] Zhao, F.; Cheng, H. H.; Zhang, Z. P.; Jiang L.; Qu, L. T. Direct power generation from a graphene oxide film under moisture. *Adv. Mater*. **2015**, *27*, 4351–4357.
[46] Jin, X. T.; Sun, G. Q.; Yang, H. S.; Zhang, G. F.; Xiao, Y. K.; Gao, J.; Zhang, Z. P.; Qu, L. T. A graphene oxide-mediated polyelectrolyte with high ion-conductivity for highly stretchable and self-healing all-solid-state supercapacitors. *J. Mater. Chem. A*. **2018**, *6*, 19463–19469.
[47] Yu, M. H.; Zhang, Y. F.; Zeng, Y. X.; Balogun, M. S.; Mai, K. C.; Zhang, Z. S.; Lu, X. H.; Tong, Y. X. Water surface assisted synthesis of large-scale carbon nanotube film for high-performance and stretchable supercapacitors. *Adv. Mater*. **2014**, *26*, 4724–4729.
[48] Haraguchi, K.; Farnworth, R.; Ohbayashi, A.; Takehisa, T. Compositional effects on mechanical properties of nanocomposite hydrogels composed of poly(N,N-dimethylacrylamide) and clay. *Macromolecules* **2003**, *36*, 5732–5741.
[49] Chen, Y. J.; Ozaki Y.; Czarnecki, M. A. Molecular structure and hydrogen bonding in pure liquid ethylene glycol and ethylene glycol–water mixtures studied using NIR spectroscopy. *Phys. Chem. Chem. Phys*. **2013**, *15*, 18694–18701.
[50] Conrad, F. H.; Hill, E. F.; Ballman, E. A. Freezing points of the system ethylene glycol-methanol-water. *Ind. Eng. Chem*. **1940**, *32*, 542–543.
[51] Spangler, J.; Davies, E. Freezing points, densities, and refractive indexes of system glycerol-ethylene glycol-water. *Ind. Eng. Chem. Anal. Ed*. **1943**, *15*, 96–99.
[52] Hu, M. M.; Wang, J. Q.; Liu, J.; Zhang, J. H.; Ma, X.; Huang, Y. An intrinsically compressible and stretchable all-in-one configured supercapacitor. *Chem. Commun*. **2018**, *54*, 6200–6203.
[53] Kumar, R. M.; Baskar, P.; Balamurugan, K.; Das, S.; Subramanian V. On the perturbation of the H-bonding interaction in ethylene glycol clusters upon hydration. *J. Phys. Chem. A* **2012**, *116*, 4239–4247.
[54] Wu, J. F.; Zhang, Q. E.; Wang, J. J.; Huang X. P.; Bai, H. A self-assembly route to porous polyaniline/reduced graphene oxide composite materials with molecular-level uniformity for high-performance supercapacitors. *Energy Environ. Sci*. **2018**, *11*, 1280–1286.
[55] Liu, N.; Su, Y. L.; Wang, Z. Q.; Wang, Z.; Xia, J. S.; Chen, Y.; Zhao, Z. G.; Li, Q. W.; Geng, F. X. Electrostatic-interaction-assisted construction of 3D networks of manganese dioxide nanosheets for flexible high-performance solid-state asymmetric supercapacitors. *ACS Nano* **2017**, *11*, 7879–7888.
[56] Hong, S.; Lee, J.; Do, K.; Lee, M.; Kim, J. H.; Lee, S.; Kim, D. H. Stretchable electrode based on laterally combed carbon nanotubes for wearable energy harvesting and storage devices. *Adv. Funct. Mater*. **2017**, *27*, 1704353.
[57] Lim, Y.; Yoon, J.; Yun, J.; Kim, D.; Hong, S. Y.; Lee, S. J.; Zi, G.; Ha, J. S. Biaxially stretchable, integrated array of high performance microsupercapacitors. *ACS Nano* **2014**, *8*, 11639–11650.
[58] Liu, Y. Q.; Zhang, B. B.; Xu, Q.; Hou, Y. Y.; Seyedin, S.; Qin, S.; Wallace, G. G.; Beirne, S.; Razal, J. M.; Chen, J. Development of graphene oxide/polyaniline inks for high performance flexible microsupercapacitors via extrusion printing. *Adv. Funct. Mater*. **2018**, *28*, 1706592.
[59] Yuan, L. Y.; Xiao, X.; Ding, T. P.; Zhong, J. W.; Zhang, X. H.; Shen, Y.; Hu, B.; Huang, Y. H.; Zhou, J.; Wang, Z. L. Paper-based supercapacitors for self-powered nanosystems. *Angew. Chem., Int. Ed*. **2012**, *51*, 4934–4938.
[60] Li, S. H.; Huang, D. K.; Zhang, B. Y.; Xu, X. B.; Wang, M. K.; Yang, G.; Shen, Y. Flexible supercapacitors based on bacterial cellulose paper electrodes. *Adv. Energy Mater*. **2014**, *4*, 1301655.
[61] Nyström, G.; Marais, A.; Karabulut, E.; Wågberg, L.; Cui Y.; Hamedi, M. M. Self-assembled three-dimensional and compressible interdigitated thin-film supercapacitors and batteries. *Nat. Commun*. **2015**, *6*, 7259.
[62] Zhao, Y.; Liu, J.; Hu, Y.; Cheng, H. H.; Hu, C. G.; Jiang, C. C.; Jiang, L.; Cao, A. Y.; Qu, L. T. Highly compression-tolerant supercapacitor based on polypyrrole-mediated graphene foam electrodes. *Adv. Mater*. **2013**, *25*, 591–595.
[63] Niu, Z. Q.; Zhou, W. Y.; Chen, X. D.; Chen J.; Xie, S. S. Highly compressible and all-solid-state supercapacitors based on nanostructured composite sponge. *Adv. Mater*. **2015**, *27*, 6002–6008.
[64] Xiao, K.; Ding, L. X.; Liu, G. X.; Chen, H. B.; Wang S. Q.; Wang, H. H. Freestanding, hydrophilic nitrogen-doped carbon foams for highly compressible all solid-state supercapacitors. *Adv. Mater*. **2016**, *28*, 5997–6002.
[65] Liang, X.; Nie, K. W.; Ding, X.; Dang, L. Q.; Sun, J.; Shi, F.; Xu, H.; Jiang, R. B.; He, X. X.; Liu, Z. H. et al. Highly compressible carbon sponge supercapacitor electrode with enhanced performance by growing nickel–cobalt sulfide nanosheets. *ACS Appl. Mater. Interfaces* **2018**, *10*, 10087–10095.
[66] Sheng, L. Z.; Chang, J.; Jiang, L. L.; Jiang, Z. M.; Liu, Z.; Wei, T.; Fan, Z. J. Multilayer-folded graphene ribbon film with ultrahigh areal capacitance and high rate performance for compressible supercapacitors. *Adv. Funct. Mater*. **2018**, *28*, 1800597.